JETS IN REAL AND VIRTUAL PHOTOPRODUCTION

H. RICK
(for the H1 Collaboration)
DESY, Notkestraße 85, D-22607 Hamburg, Germany. rick@mail.desy.de

Measurements of jet cross sections from real and virtual photon-proton scattering are presented, based on recent results from the H1 experiment at HERA. For the case of real photoproduction, differential cross sections of di-jet events are shown as a function of the transverse energy of the jets and the reconstructed momentum fraction of the struck parton from the photon. Based on these cross sections, an effective leading order parton density of the photon is extracted as a function of the transverse momentum scale of the jets. In virtual photoproduction, single inclusive jet cross sections are presented as a function of the jet transverse energy and the photon virtuality.

1 Introduction

HERA's electron beam is accompanied by a flux of real and virtual photons whose partonic structure reveals itself via the formation of jets with large transverse momentum when scattering off the constituents of the proton. The large center of mass energy and the wide range of energies and virtualities of these photons make the HERA collision experiments a unique opportunity to study the hadronic structure of the photon as well as its dependence on the two scales p_{T}^2 and Q^2 which represent the squared transverse momentum in the partonic process and the photon virtuality.

The first of the two analyses presented here investigates the p_{T}^2 dependence of the jet cross section and the parton distribution of quasireal photons at $Q^2 \approx 0$, while the second analysis deals with the Q^2 evolution of the virtual photon–proton jet cross section in bins of the transverse jet energy.

1.1 Experimental setup

A detailed description of the H1 detector can be found in [1]. In the analyses presented here, hadronic jets are identified in the H1 liquid argon calorimeter, which covers polar angles between 4° and 150° with respect to the proton beam direction. The scattered electron in virtual photon-proton scattering events and part of the hadronic final state at angles larger than 150° is seen in the backward electromagnetic calorimeter. In the case of real photoproduction, the scattered electron escapes unseen by the central detector through the beam hole. The signals from the tracking detectors inside the calorimeter system are used for reconstructing the position of the interaction vertex and to support the calorimetric measurement of the hadronic energy flow.

The data used for these analyses were taken during the 1994 run period with an integrated luminosity of $2.9\,\mathrm{pb}^{-1}$. For the analysis of virtual photon–proton scattering the event sample was complemented by a special run of $120\,\mathrm{nb}^{-1}$ which was taken in 1995 with the interaction vertex shifted by 70 cm with respect to the nominal vertex position, extending the acceptance of the backward calorimeter for the scattered electron down to photon virtualities of $Q^2 = 0.65\,\mathrm{GeV}^2$.

2 Di-jets in real photoproduction

In the following analysis of di-jet events from real photoproduction, jets were found by a cone algorithm [2] using a cone with radius R=0.7 in the plane of azimuthal angle ϕ and pseudorapidity η. Events were accepted in which at least 2 jets were found with transverse energies above 8 GeV each. The two jets with the highest transverse energies found in an event were used for approximate reconstruction of the kinematics of the underlying partonic process.

The cross section as a function of the parton momentum fraction in the photon x_γ and the transverse momentum p_{T} of the jets was corrected in a two-step procedure. In a first step, the data were corrected for the smearing of the detector in order to obtain the cross section for di-jet production. This cross section was then corrected further for effects of fragmentation, higher order parton radiation and underlying event energy in order to extract the leading order parton density in the photon.

2.1 Differential di-jet cross sections

The double-differential cross section for di-jet production as a function of the reconstructed parton momentum fraction in the photon x_γ^{jets} and the transverse energy E_T of the second highest E_T jet in the event is shown in figure 1. The result is given as an ep cross section for the kinematic region defined by the cuts that are listed in the figure caption. The error bars include the full systematic error which is dominated by the uncertainty in the calibration of the calorimeter for hadronic energy measurement. This error is between 15% and 30% of the cross section, with the largest uncertainty occurring in the lowest x_γ^{jets} bins. A variation of the parameters of the two-dimensional unfolding procedure [3] which was used for correcting the data causes an uncertainty below 10%, and the uncertainty in the determination of the triggering efficiency for jet events contributes another 10% to the relative systematic error.

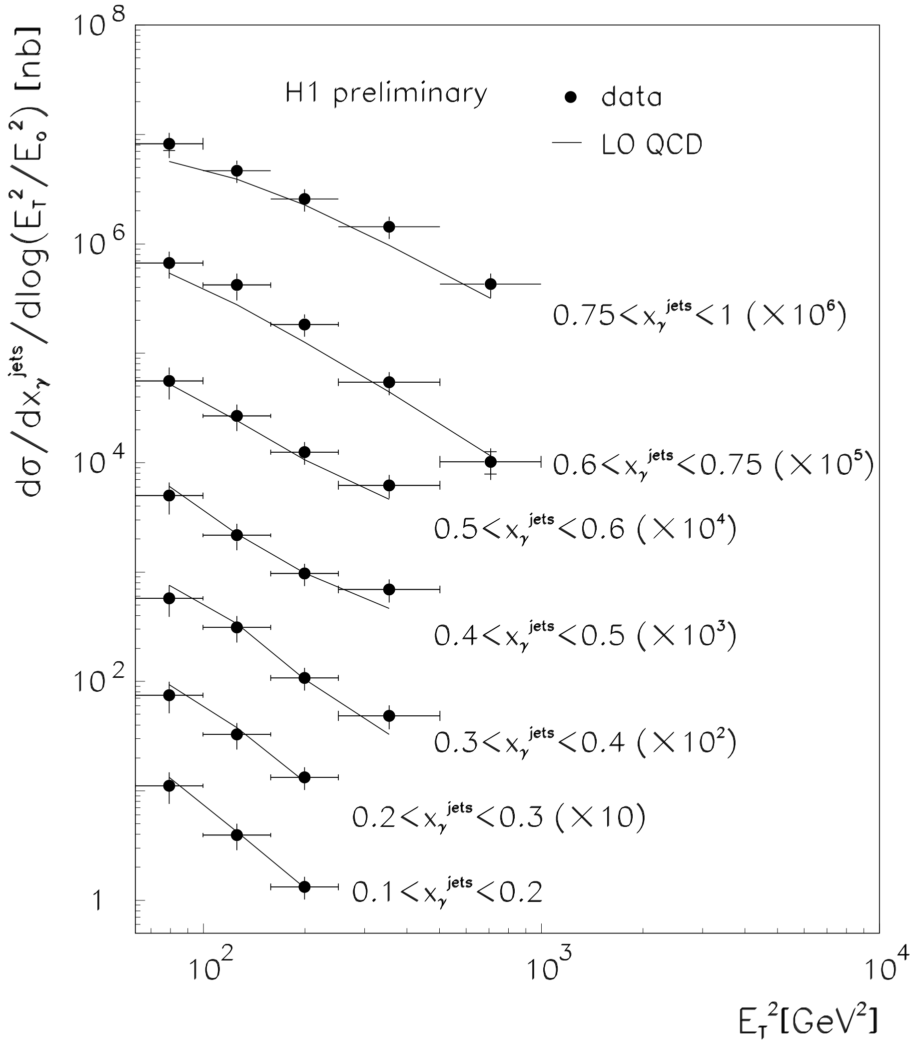

Figure 1: Double-differential di-jet cross section from photoproduction of real photons. Jet finding is based on the hadronic final state using a cone algorithm with a cone radius of 0.7 units in the plane of pseudorapidity η and azimuthal angle φ. The cross section is given as a function of the logarithm of the squared transverse energy $\log(E_T^2/E_0^2)$ ($E_0 = 1\,\mathrm{GeV}$) of the jet with the second highest E_T, in bins of the parton momentum fraction in the photon which was reconstructed from the transverse energies (E_{T1},E_{T2}) and pseudorapidities (η_1,η_2) of the two jets: $x_\gamma^{\mathrm{jets}} = (E_{T1}e^{-\eta_1} + E_{T2}e^{-\eta_2})/(2yE_e)$. The jet pseudorapidities were restricted to the range $-0.5 < \eta_{1,2} < 2.5$ and $|\eta_1 - \eta_2| < 1$ in the HERA laboratory system. The scaled photon energy in units of the incoming electron energy $y = E_\gamma/E_e$ was required to be in the range $0.2 < y < 0.83$, and the photon virtuality Q^2 was below $Q^2 = 4\,\mathrm{GeV}^2$.

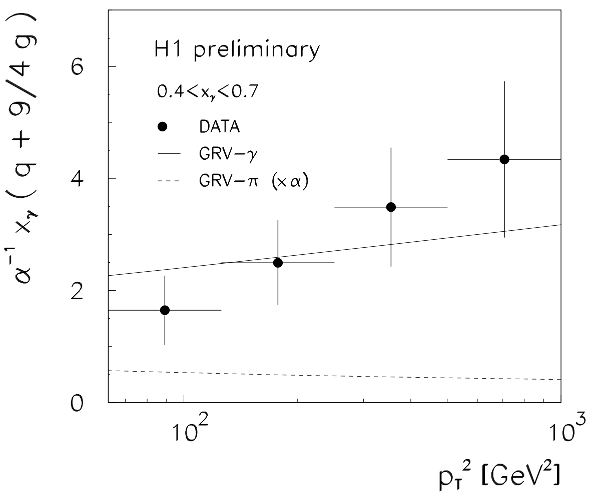

Figure 2: The effective photon parton distribution $x_\gamma \tilde{f}(x_\gamma, p_{\mathrm{T}}^2) = x_\gamma(q(x_\gamma, p_{\mathrm{T}}^2) + 9/4\, g(x_\gamma, p_{\mathrm{T}}^2))$ is shown as a function of the transverse momentum scale p_{T}^2, averaged over parton momentum fractions in the range $0.4 < x_\gamma < 0.7$. The data (black dots with error bars) are compared to the GRV parameterisation of the photon (full curve) and the pion (dashed, scaled by a factor α).

In figure 1 the measured cross section is compared to the prediction of the PYTHIA [4] generator using the GRV [5] parameterisations of the photon and proton parton distributions. The comparison shows reasonable agreement between the model and the data over the whole range of x_γ^{jets} and E_T shown, with some possible deviations in the region of large x_γ^{jets} where the photon parton distribution is not well constrained from previous measurements.

2.2 The effective parton density of the photon

In contrast to measurements of the photon structure function F_2 at e^+e^- experiments, which corresponds to a sum over the quark densities in the photon, resolved photon processes at HERA are sensitive to both the quark and the gluon [6] densities in the photon. In this jet analysis however, jets originating from final state quarks cannot be distinguished experimentally from those originating from gluons, so that quark and gluon densities cannot be determined separately. Therefore the so-called **S**ingle **E**ffective **S**ubprocess approximation [7] is used here, which implies the definition of an effective parton distribution of the photon $\tilde{f}^\gamma(x_\gamma, p_{\mathrm{T}}^2) = \sum_q (q^\gamma(x_\gamma, p_{\mathrm{T}}^2) + \bar{q}^\gamma(x_\gamma, p_{\mathrm{T}}^2)) + \frac{9}{4} g^\gamma(x_\gamma, p_{\mathrm{T}}^2)$. Here q^γ and g^γ are the quark and gluon parton densities in the photon. The sum runs over all quark flavours, the factor $\frac{9}{4}$ represents the strength of the gluon-gluon coupling relative to the gluon-quark coupling. With this definition, the differential di-jet cross section as a function of the parton momentum fractions x_γ and $x_{\rm p}$ in photon and proton, the scaled photon energy in units of the incident electron energy $y = E_\gamma / E_e$ and the scattering angle θ^* of the final state partons in their center of mass frame with respect to the beam axis factorizes approximately as follows:

$$\frac{d^4\sigma}{dy\, dx_\gamma\, dx_{\rm p}\, d\cos\theta^*} \approx \frac{1}{32\pi s_{\rm ep}} \frac{f_{\gamma/{\rm e}}(y)}{y} \frac{\tilde{f}_\gamma(x_\gamma, p_{\rm T}^2)}{x_\gamma} \frac{\tilde{f}_{\rm p}(x_{\rm p}, p_{\rm T}^2)}{x_{\rm p}} |M_{\rm SES}(\cos\theta^*)|^2$$

In this expression, $f_{\gamma/{\rm e}}$ is the photon flux of the beam electron, $\tilde{f}_\gamma$ and $\tilde{f}_{\rm p}$ are the effective parton densities of photon and proton, and $M_{\rm SES}$ is the matrix element for the effective subprocess, which can be approximated by the matrix element for the process $qq' \to qq'$ with a t-channel gluon exchange.

In order to extract the effective parton density of the photon $\tilde{f}_\gamma(x_\gamma, p_{\rm T}^2)$ from the data, the corrected di-jet cross section given in the previous paragraph was corrected to the parton variables x_γ and $p_{\rm T}$ in a second unfolding step. For estimation of the model dependent uncertainties which are inevitably introduced by an interpretation of the data in terms of a leading order model, this last step was repeated several times using PYTHIA simulations with different parameter settings, or the simulation of the PHOJET [8] generator. The difference between the models tested mainly concerns variations of the underlying event energy as modelled by multiple parton interactions, and of higher order QCD effects, which are modelled by a parton shower mechanism. A more detailed discussion of these effects is given in [9] and [10]. In the region around $x_\gamma \approx 0.5$, the variation of the result with these alternative models is around 10% of the parton density.

The unfolded effective parton density of the photon is shown in figure 2 as a function of the squared transverse momentum transfer $p_{\rm T}^2$ in the hard scattering process, and averaged over parton momentum fractions in the range $0.4 < x_\gamma < 0.7$. The parton density is compared to the effective photon parton density which was calculated from the GRV parameterisation. As an approximation of the vector meson dominance model of the photon, the GRV pion parton density is also shown, scaled by the factor α. The measured parton density shows a rise with the transverse momentum scale $p_{\rm T}^2$ which is clearly different from the pion curve both in shape and in absolute rate. This difference between the photon and typical hadrons is caused by the pointlike coupling of the photon to quark-antiquark-pairs. It has been observed in measurements of the photon structure function F_2 at e^+e^- experiments (e.g., [11]), and is here now directly verified for the first time in photoproduction at an ep experiment.

H1 Preliminary

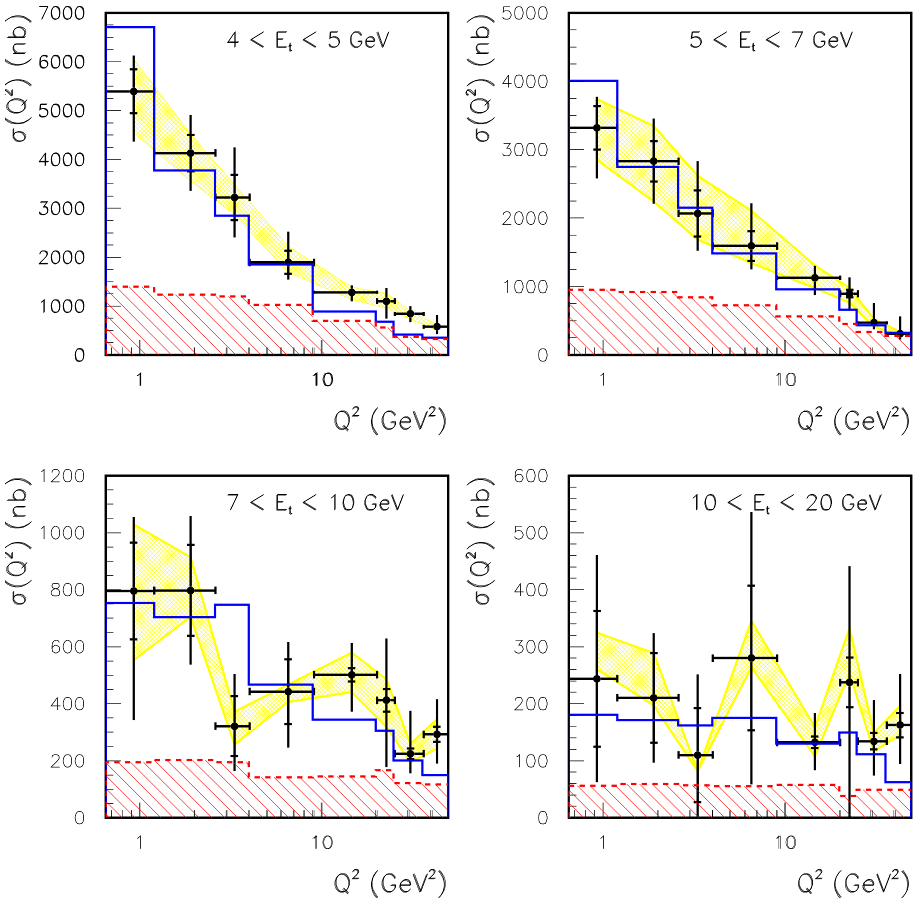

Figure 3: Single inclusive jet cross section from virtual photoproduction as a function of the photon virtuality Q^2, in bins of the jet transverse energy E_t. Jets were found in the pseudorapidity range $-2.5 < \eta^* < -0.5$ in the photon–proton center of mass frame, using a $\mathrm{k_T}$ clustering algorithm. The data are presented as γp cross sections, normalized to the flux of virtual photons that are radiated off the beam electron in the y range $0.3 < y < 0.6$. The data points are shown with statistical errors (inner error bars) and the quadratic sum of statistical and systematic errors (full error bars) and are compared to the prediction of the HERWIG model with the direct photon component only (hatched histogram) and the sum of direct and resolved contributions (full line). The shaded band indicates the systematic error induced by the uncertainty in the calibration of the calorimeter.

3 Jets in virtual photoproduction

For the case of virtual photons, resolved-photon processes are expected to dominate the jet production cross section as long as the transverse energy scale E_t of the jets is much larger than the virtuality of the photon Q^2 ($E_t^2 \gg Q^2$), while they become more and more suppressed with increasing Q^2. In the limit $Q^2 \gg E_t^2$ the cross section can be described by the classical deep-inelastic scattering picture of a pointlike photon. This behaviour is verified in the following virtual photon analysis, which is based on jets found by a $k_{\rm T}$ clustering algorithm in the virtual photon–proton center of mass frame. Figure 3 shows the single inclusive jet cross section as a function of the photon virtuality Q^2, in bins of the jet transverse energy E_t. The cross section is shown as a γp cross section, corrected for detector effects, and divided by the flux of virtual photons from the incident electron. It is compared to the prediction of the virtual photon–proton model of the HERWIG [12] generator which implements a continuous suppression of the resolved photon component with increasing Q^2. The pure pointlike, direct photon component, which is shown separately as hatched histograms, is not sufficient to describe the measured jet rate, while the complete model including the resolved part gives a much better prediction of the jet cross section both in shape and absolute normalisation.

This preliminary result already gives an indication for a resolved contribution even at large photon virtualities $Q^2 \gg 0$. The next step for future studies in this interesting field could consist in a direct reconstruction of the underlying parton kinematics in order to measure the parton distribution in virtual photons in a similar way as it is being done for the real photon.

References

1. H1 Collab., I. Abt *et al*, *Nucl. Instrum. Methods* A **386**, 310 (1997).
2. J. Huth *et al*, Fermilab-Conf-90/249-E (1990).
3. G. D'Agostini, *Nucl. Instrum. Methods* A **362**, 487 (1995).
4. T. Sjöstrand, *Comput. Phys. Commun.* **82**, 74 (1994).
5. M. Glück, E. Reya, A. Vogt, *Z. Phys.* C **53**, 127,651 (1992).
6. H1 Collab., T. Ahmed *et al*, *Nucl. Phys.* B **445**, 195 (1995).
7. B.L. Combridge, C.J. Maxwell, *Nucl. Phys.* B **239**, 429 (1984).
8. R. Engel, J. Ranft, *Phys. Rev.* D **54**, 4244 (1996).
9. H1 Collab., S. Aid *et al*, *Z. Phys.* C **70**, 17 (1996).
10. M. Erdmann, "The Partonic Structure of the Photon", Springer Tracts in Mod. Phys. 138, Berlin, Springer (1997).
11. AMY Collab., S.K. Sahu *et al*, *Phys. Lett.* B **346**, 208 (1995).
12. G. Marchesini *et al*, *Comput. Phys. Commun.* **67**, 465 (1992).